

Voltage control in low voltage grids with independent operation of on-load tap changer and distributed photovoltaic inverters

Original

Voltage control in low voltage grids with independent operation of on-load tap changer and distributed photovoltaic inverters / Spertino, F.; Ciocia, A.; Mazza, A.; Nobile, M.; Russo, A.; Chicco, G.. - In: ELECTRIC POWER SYSTEMS RESEARCH. - ISSN 0378-7796. - 211:(2022), p. 108187. [10.1016/j.epsr.2022.108187]

Availability:

This version is available at: 11583/2969159 since: 2022-06-30T16:59:45Z

Publisher:

Elsevier Ltd

Published

DOI:10.1016/j.epsr.2022.108187

Terms of use:

This article is made available under terms and conditions as specified in the corresponding bibliographic description in the repository

Publisher copyright

Elsevier postprint/Author's Accepted Manuscript

© 2022. This manuscript version is made available under the CC-BY-NC-ND 4.0 license
<http://creativecommons.org/licenses/by-nc-nd/4.0/>. The final authenticated version is available online at:
<http://dx.doi.org/10.1016/j.epsr.2022.108187>

(Article begins on next page)

18 **Abstract:** This paper aims to find the optimal setups of voltage control devices in different
19 configurations of Low Voltage (LV) grids with strong PhotoVoltaic (PV) diffusion by
20 performing dedicated simulations. Distributed PV inverters and On-Load Tap Changer (OLTC)
21 are simulated without considering their coordination, to avoid large investments in new
22 communication infrastructures. Thus, each device independently works to decrease voltage
23 deviations in the respective grid connection point. PV generation and consumption profiles are
24 measured and used in two simulated LV grids, connected to the Medium Voltage (MV) grid by
25 a MV/LV transformer with rated powers of 400 and 250 kVA, respectively. The calculation of
26 the optimal devices setups is addressed as a multi-objective problem, considering objectives of
27 voltage quality, grid losses, and OLTC lifespan increase. Multiple simulations are performed
28 by varying the setup of the voltage controls, and considering different positioning and sizes of
29 the generators. In the hardest case, the ratio between the maximum PV power generation and
30 the maximum load in the whole grid is $\approx 70\%$. Pareto analysis is carried out to find the non-
31 dominated solutions and TOPSIS is applied to rank the solutions. Finally, a sensitivity analysis
32 is performed by changing the weights attributed to each objective function.

33

34 **Keywords:** Voltage control, low voltage grid, photovoltaic system, reactive power, on-load tap
35 changer, Pareto front, sensitivity analysis, TOPSIS method.

36

37 **1. Introduction**

38 In the last decades, the increase of distributed generation in Low Voltage (LV) distribution grids
39 lowered the energy production dependence from the centralized power plants. The number of
40 distributed renewable energy systems, mainly PhotoVoltaic (PV) generators, is increasing,
41 supporting the reduction of greenhouse gas emissions. Due to the fluctuations of solar
42 irradiance, PV generation is highly variable and may lead to voltage fluctuations, reverse power

43 flows and power quality issues [1][2].

44 A general method to reduce voltage violations in LV grids calls for grid investments from the
45 Medium Voltage (MV) connection point, e.g., with replacement of the MV/LV transformer
46 and/or the reduction of the cable impedances [3]. However, these solutions are costly and only
47 partially effective and hence, with larger and larger share of distributed generation (mainly PV
48 systems), the LV grid operation will require more advanced voltage control techniques.

49 In the literature, many articles describe various methods to perform voltage control. It is clearly
50 established that both centralized and local voltage controls have to be simultaneously present
51 to ensure more options for effective voltage control. For centralized control, one of these
52 methods involves the operation of the On-Load Tap Changer (OLTC), which modifies the tap
53 position of the transformer to reach the voltage target. This device is mainly used on the High
54 Voltage (HV) side of the HV/MV transformers, for controlling voltage in the MV grid.
55 However, in recent years, it is also being used in LV grids [4]. For example, the unbalanced
56 MV electrical grid (IEEE-123 nodes), characterized by a significant presence of PV generators,
57 is analyzed in [5]. The control is carried out by OLTC and PV inverters that provide inductive
58 or capacitive reactive power. In some cases, the voltage variation at the node with OLTC can
59 cause voltage violations, especially in the nodes with high generation and low load. In this case,
60 distributed control is fundamental because it acts locally at the node where the violation occurs
61 [3]. It is noted that in [5] there is a communication system between inverters and the OLTC.
62 With respect to [5], the MV grid analyzed in [6] is divided into several zones, each one equipped
63 with an autotransformer and/or other devices, such as Capacitor Banks (CB), static reactive
64 power compensators (STATCOM) and/or PV inverters. The logic for the reactive and active
65 power control aims to minimize the number of tap changes of the OLTC by regulating more
66 with other devices. Nevertheless, the study is based on the use of a communication system
67 between the devices to perform real-time coordinate voltage control.

68 The IEEE 123-node MV grid is used in [7], with voltage control devices, such as Static Var
69 Compensator (SVC) and OLTC, which communicate to improve voltages. The goal is to
70 minimize different objective functions (total grid losses, number of tap changes, and SVC
71 wear). To solve this multi-objective problem, a weight is assigned to each objective function.
72 By changing the weights, the performance of each different control is discussed. In [8], the
73 voltage is regulated by inverters that provide inductive or capacitive reactive power to stabilize
74 the voltage at the Point of Common Coupling (PCC). They interact via a real-time
75 communication system. Proportional Integral (PI) regulators are used to provide closed-loop
76 voltage control between the grid and PV systems and make the control faster and more efficient.
77 In [9], the voltage is regulated via PV inverters providing reactive power; PI regulators are used
78 for the control logic, to decrease the voltage deviation and try keeping the losses low. In this
79 case, centralized devices are not considered.

80 In [10], a mixed control is performed, with a coordination system among distributed and
81 centralized devices. In particular, the grid is divided into several zones, each consisting of a
82 certain number of cascaded devices. A ZIP-type load model is used, and the volt-var
83 optimization method allows to reduce the number of tap changes. Three objective functions are
84 defined, related to the number of tap changes, the Step Voltage Regulator (SVR) wear, and the
85 generated active power. The first two objective functions are minimized, while the third one is
86 maximized. From the results obtained, a decrease of the voltage deviation is due to the number
87 of tap changes executed. Moreover, storage systems are used to improve the control
88 performance. The MV grid in [11] is divided into zones, each of them is equipped with control
89 devices (inverter, OLTC, CB and SVR). With respect to other papers, there is no
90 communication system, every device is independent of others and regulates only the voltage in
91 its PCC, and the distributed inverters use reactive power to control voltage.

92 Another method to control voltage in LV grids with high PV generation is the Active Power

93 Curtailment (APC) [12]. It consists of the reduction of active power generated to reduce the
94 voltage at the PCC. In particular, there are two different approaches: in the first one, all inverters
95 have the same reduction logic; in the second one, the setups are different. From the results
96 obtained in [12], in the second approach a lower voltage deviation is obtained than in the first
97 one, but with more Joule losses. The APC method is more efficient if there is a coordination
98 between devices [13]. In the absence of a communication system, it is more convenient to
99 regulate by providing only reactive power. In this way, the active power does not change, and
100 the energy produced is maximized, as described in [14] and [15]. In these two works, the control
101 is performed only by PV inverters that provide inductive or capacitive reactive power. The
102 reactive and APC method can be combined, as in [12] and [16].

103 Furthermore, Battery Energy Storage Systems (BESS) can be used to increase the control
104 effectiveness [16][17]. In [18] and [19], BESS and PV inverters are used to control voltage. In
105 particular, in [20] each PV system is equipped with BESS which store energy only when the
106 active power generated is greater than a threshold. This solution leads to a reduction of the
107 voltage deviation. The work [19] studies how the control performance changes according to the
108 characteristics of the grid. In urban grids characterized by relatively short distribution lines and
109 non-negligible transformer parameters, with low R/X ratio (about 1), the reactive power
110 provided by PV inverters is sufficient to adjust the voltage effectively. Instead, in rural grids
111 characterized by longer distribution lines and higher R/X ratio (about 4÷5), it is advisable to
112 regulate the voltage using PV inverters and BESS. The drawbacks of these last two works are
113 the high cost of BESS and the absence of centralized devices. A solution that considers the costs
114 in the optimization of LV distribution networks with OLTC, PV inverters and BESS is proposed
115 in [20].

116 With respect to the analyzed papers, the present work does not consider coordination systems,
117 and each device regulates the voltage independently and for each phase. Moreover, to maximize

118 the use of renewable sources, it is not considered the possibility to reduce the active power
119 generated to mitigate the voltage issues. No BESS is included, to avoid the related costs. The
120 present paper improves the work in [21], by describing in detail a more advanced procedure to
121 perform the voltage control using centralized and distributed devices. In addition, Pareto
122 analysis and TOPSIS are used to calculate the optimal setups of all the control devices. A
123 sensitivity analysis is added to study the results variation as a function of the weights of the
124 multi-objective problem. Finally, the whole procedure is applied to two different LV grids and
125 results are discussed.

126 The next sections of this paper are organized as follows. Section 2 describes the voltage control
127 methods. Section 3 describes the proposed procedure to find the optimal setups of the PV
128 inverters and OLTC for the voltage control. Section 4 presents the case studies. Section 5 shows
129 the simulation results. The last Section contains the conclusions.

130

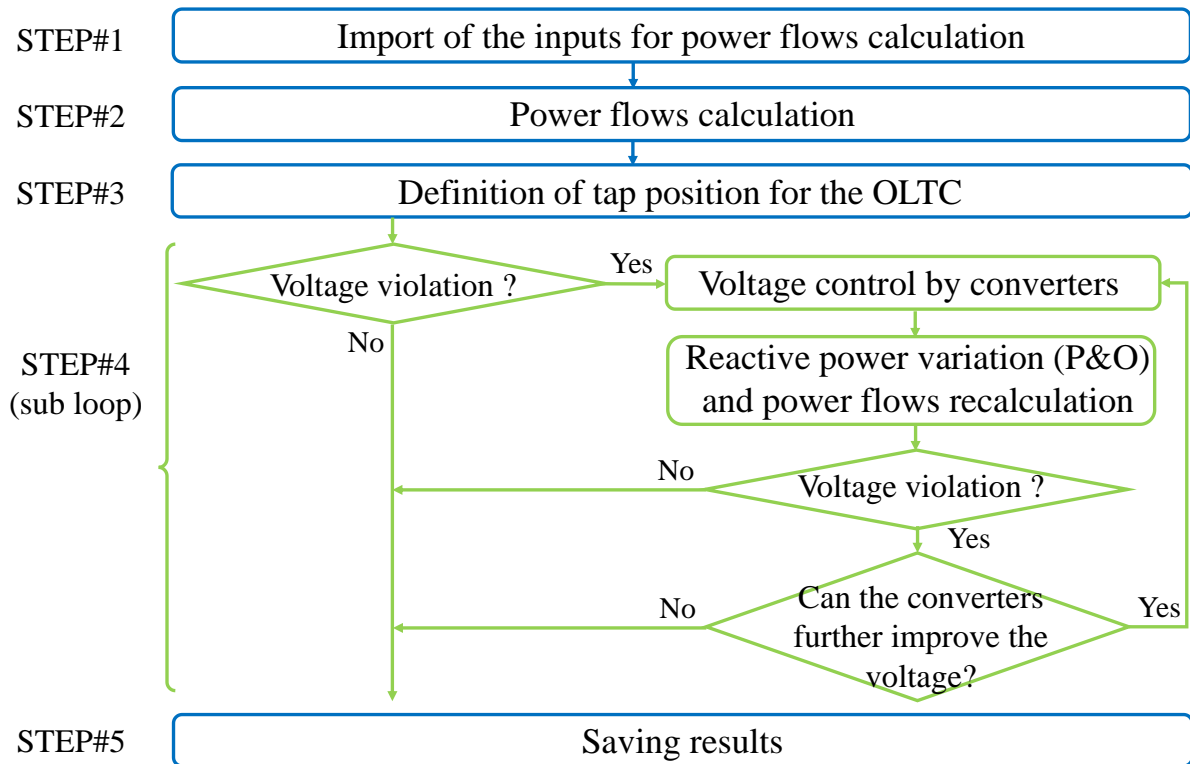
131 **2. Simulation of voltage control solutions**

132 The various aspects of simulating the voltage control by considering centralized and distributed
133 Voltage Control Devices (VCDs) are addressed below. Section 2.1 describes the procedure used
134 to simulate the operation of a LV grid with VCDs, i.e., an OLTC and distributed PV inverters.

135 After the general description of the whole procedure, Section 2.2 presents the details about the
136 proposed logic for the voltage control performed by distributed PV inverters, that is, based on
137 voltage criteria, voltage limits, and the logic to reach the optimal reactive power. Finally,
138 Section 2.3 presents the logic used to perform voltage control by OLTC, showing the details of
139 the procedure for the simulation of the OLTC operation and presenting a simple example of the
140 effect of changing the setup parameters of the OLTC.

141 *2.1 Voltage control by centralized and distributed devices*

142 Fig. 1 shows the flowchart of the whole procedure to calculate the power flows and simulate
 143 the voltage control for both centralized and distributed VCDs. Assuming steady state condition,
 144 the procedure is repeated for each time step, which in the present work is 1 minute. The time
 145 step of 1 min is typical for steady-state simulations for voltage control analysis [22][23][24]. It
 146 permits to avoid the detailed modelling of dynamic processes of the equipment involved in the
 147 voltage control. For example, in case of the OLTC equipped with transition resistors, the
 148 transition between the resistors causes the current to vary during the switching process. In
 149 particular, winding inductance, contact resistance and contact movement, interruptions and
 150 arcing may affect the current amplitude [25][26]. The total operation time of an OLTC is
 151 between few seconds to tens of seconds, depending on the respective design [27]. On these
 152 bases, the time step of 1 min is sufficiently long to avoid the need of representing the dynamics
 153 of the tap changers, which are faster.



154

155 Fig. 1. Procedure for power flows calculation and voltage control performed for each 1-min time step
 156 of the simulation.

157 The procedure is composed of the following steps:

- 158 • STEP#1: the inputs for power flow calculation (e.g., grid data, generation and load
159 profiles, capability curves, parameters of the controllers, voltage limits) are imported.
160 From the second minute onwards, the inputs include the OLTC tap position, and the
161 updated parameters of the OLTC proportional-integral control.
- 162 • STEP#2: a first power flow calculation is performed for time step t without change in the
163 voltage control, with respect to the previous time step $t-1$. The Backward Forward Sweep
164 (BFS) method is performed in the three-phase unbalanced LV grid. The equations to
165 calculate the voltages and currents are indicated in [28]. The detailed procedure for power
166 flow calculation and voltage control works according to [29].
- 167 • STEP#3: the tap position of the OLTC is calculated, according to the PI control described
168 in Section 2.3.
- 169 • STEP#4: it consists of a sub-loop that can be run several times for each time step. A check
170 of voltage violation for each node of the grid with a PV inverter is performed. In case of
171 violation, the power flows are recalculated with the BFS by considering new reactive
172 power quantities according to a logic which looks for the best quantity of reactive power
173 to inject/absorb. The PV inverter continues to regulate, and simulations are repeated until
174 there is no voltage violation, and not even one inverter can further improve the voltage
175 (i.e., all control criteria are satisfied). The criteria that define if the inverters cannot further
176 improve the voltage resulting in the exit from this sub-loop, and the logic to regulate
177 reactive power, are described in Section 2.2.
- 178 • STEP#5: in absence of voltage violations or control possibility, the procedure exits from
179 the loop, and data are saved.

180 The previously described procedure is repeated for each time step. At the end of the simulations,
181 the losses and voltage indicators are calculated to compare the results obtained for different
182 setups of the devices. All the calculations in this paper are performed by a Matlab[®] code written

183 by the authors.

184 2.2 Voltage control by distributed PV inverters

185 In case of voltage violations, the PV inverters provide inductive or capacitive reactive power to
186 keep the voltage within the limits. In different countries, the standards require that the PV
187 inverters can provide reactive power to support the grid operation. For example, the Italian
188 standard CEI 0-21 used for LV grids [30] defines two capability curves depending on the rated
189 active power P_{rated} of the PV system. The feasible operation region for the active and reactive
190 power generated is located inside the corresponding capability curve. The numerical threshold
191 on P_{rated} is determined by considering the rated voltage $V_{\text{rated}} = 400$ V, the rated current $I_{\text{rated}} =$
192 16 A, and the power factor $PF = 1$, so that $P_{\text{rated}} = \sqrt{3} V_{\text{rated}} I_{\text{rated}} PF_{\text{ref}} = 11.08$ kW. The
193 formulation of the maximum power for the two capability curves is based on the reference
194 power factor $PF_{\text{ref}} = 0.9$:

195 1) If $P_{\text{rated}} \leq 11.08$ kW, the maximum reactive power depends on the active power
196 generated P , as $Q_{\text{max}}(P) = P \text{tg}(\arccos(PF_{\text{ref}}))$, so that the power factor never decreases
197 below the limit PF_{ref} [30].

198 2) If $P_{\text{rated}} > 11.08$ kW, the maximum reactive power Q_{max} is constant and is determined as
199 $Q_{\text{max}} = P_{\text{rated}} \text{tg}(\arccos(PF_{\text{ref}})) = 0.484 P_{\text{rated}}$, independently of the active power generated.

200 In both cases, the capability curves are symmetrical with respect to the reactive power, so that
201 the minimum reactive power is $Q_{\text{min}}(P) = -Q_{\text{max}}(P)$ in the first case and $Q_{\text{min}} = -Q_{\text{max}}$ in the
202 second case.

203 As previously mentioned, in the present work there is no communication system, and each PV
204 inverter manages reactive power independently of the others [31][32]. This logic is created to
205 simplify the real implementation of Voltage Control Devices (VCDs) in actual grids. In fact,
206 the whole procedure is based on the comparison between the voltage measured by the device

207 in its connection point and voltage limits. Each VCD does not require communication, because
208 each device works autonomously, without cooperating with a centralized VCD (e.g., an OLTC)
209 or other distributed VCDs. In a real implementation, the devices do not need to know advanced
210 information about the grid, such as the number of nodes, the number of lines and the related
211 impedances, etc. In fact, the VCDs operate only on the basis on the local information (the power
212 flow is not calculated by VCDs). As a result, the VCDs logics do not change in case of the
213 installation of additional distributed generation, or in case of changes in the grid configuration,
214 which modify the impedance seen from the point of connection of the VCD.

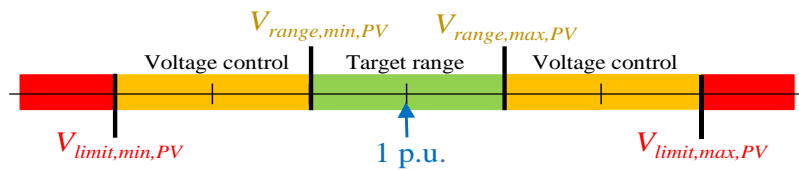
215 *2.2.1 Perturb & Observe technique for voltage control*

216 The control of one device can improve voltage in its node and can affect the other nodes. In this
217 paper, the logic used to calculate the best reactive power quantity is based on the Perturb &
218 Observe (P&O) technique. It is a logic widely used to obtain the maximum power point of the
219 DC side of the PV inverters [33]. The principle of operation of the original P&O is briefly
220 described with the following example. A PV inverter is working at a DC voltage power level
221 defined by environmental conditions (irradiance and temperature). To reach the maximum
222 output, the PV inverter increases the DC voltage of the PV modules and measures the new DC
223 power production. If the production increases, the increase is repeated until there is no
224 significant improvement of the power output. On the contrary, if the change in the DC voltage
225 leads to a decrease of the output power, the procedure will be repeated in the opposite direction,
226 i.e., by reducing the DC voltage [34]. In the present work, a similar P&O is used. The reactive
227 power is changed to reduce the voltage deviation, i.e., the difference between the voltage
228 measured at point of connection of the PV inverter with the grid and the reference voltage equal
229 to 1 per unit (p.u.). In case of voltage violation, reactive power is added (capacitive for
230 undervoltage, inductive for overvoltage): the electronic circuits in the PV inverter increase or
231 decrease (with its sign) the phase angle between current and voltage to change the reactive

232 power injected or absorbed. If the voltage violation is reduced but not solved, the inverter
 233 increases its reactive power. If the change in reactive power does not lead to a voltage
 234 improvement, the control ends to avoid an unnecessary increase of the total Joule losses L_{tot} .

235 2.2.2 Voltage limits

236 The setup of the voltage control is changed by modifying the limits shown in Fig. 2 [29]:



237

238 Fig. 2. Voltage limits for the PV inverters contributing to voltage control

239 The inverters do not provide reactive power when the voltage is included in the range
 240 $V_{range,min,PV} - V_{range,max,PV}$. If the voltage is between $V_{range,min,PV}$ and $V_{limit,min,PV}$ or between
 241 $V_{range,max,PV}$ and $V_{limit,max,PV}$, the inverter works to correct the voltage violation. In case of
 242 overvoltage ($V_i > V_{range,max,PV}$), the inverters provide inductive reactive power to reduce the
 243 voltage. The proposed voltage control could work also in case of larger violations, i.e., the red
 244 areas in Fig. 2 corresponding to a voltage lower than $V_{limit,min,PV}$ or higher than $V_{limit,max,PV}$.
 245 Nevertheless, in these cases, the voltage control is stopped to avoid interactions with other
 246 logics included in the real applications. In fact, according to different grid codes [30][35], the
 247 inverters have other tasks to perform: grid codes require the PV systems to provide low voltage
 248 ride-through (LVRT) capability, i.e., the ability to withstand the abnormal voltage and remain
 249 grid-connected in the event of grid failures [36]. The timing of LVRT is about hundreds of
 250 milliseconds, very fast with respect to the time steps considered in this paper, and if the voltage
 251 remains outside the limits for a longer period there is the disconnection of the PV inverter from
 252 the grid, operated by the protection systems. As such, voltage control is active only inside the
 253 voltage control ranges indicated in Fig. 2. A detailed discussion on LVRT capability is out of
 254 scope for this paper.

255 2.2.3 Voltage control criteria

256 In the sub-loop described in the previous subparagraph, corresponding to STEP#4 in Fig. 1, at
257 every iteration, each inverter has to respect a set of criteria to manage its reactive power. These
258 criteria are used to guarantee the correct operation of the inverters and avoid useless reactive
259 power in the grid. The individual inverters are not influenced by the criteria applied to the other
260 devices and can be stopped in controlling voltage during an iteration, and restart in the next
261 iteration. For example, let us suppose that, at the first iteration, an inverter in a generic node#A
262 does not provide reactive power, because there is no violation in its PCC, but an increase in the
263 reactive power injection in other nodes leads to a violation in node#A. Thus, the inverter in
264 node#A will work to adjust its voltage until all its criteria are satisfied.

265 The criteria are:

- 266 • *Usefulness criterion*: if the voltage difference $V_i^{(k)} - V_i^{(k-1)}$ between two iterations (k and
267 $k-1$) is less than a threshold ($V_i^{(k)} - V_i^{(k-1)} < \varepsilon$), the inverter stops the control to avoid a
268 useless increase of the losses L_{tot} . A low value of ε makes the inverters to use all their
269 reactive power. This threshold permits the inverters, that cannot significantly contribute
270 to the improvement of voltage profiles, to exit from the loop.
- 271 • *Consistency criterion*: there is an inconsistency if the inverter provides inductive power
272 and its PCC voltage increases, or if it provides capacitive power and the voltage
273 decreases. The reason is that in these cases the control of the voltage is useless; voltage
274 variation is dominated by other devices in the grid (for example another PV generator
275 with a much higher power in a close node). In these cases, the inverter stops the reactive
276 power variation.
- 277 • *Saturation criterion*: when the inverter exceeds the maximum reactive power according
278 to its capability curve, it saturates and stops the control. Obviously, if a reactive power
279 reduction is required, the inverter applies it.

280 2.3 Voltage control performed by OLTC

281 Centralized voltage control by On Load Tap Changer (OLTC) is based on PI control [29]. By
282 changing the tap, the goal of the control is to keep the voltage at the LV side of the transformer
283 as close as possible to the target voltage V_{target} . A key parameter of this control is the over-under
284 voltage counter $\alpha_{\text{OLTC}}(t)$. The procedure to control the OLTC is shown in the flowchart in Fig.
285 3:

- 286 • STEP# α : the data from the previous time step $t-1$ are imported. They are the updated
287 voltage counter $\alpha_{\text{OLTC}}(t-1)$, and the tap position to be used in time step t .
- 288 • STEP# β : simulations are performed for time step t . From all the results (currents,
289 voltages, power flows, losses, etc.), it is calculated the deviation ΔV_{OLTC} between the
290 simulated voltage at the LV side of the transformer V_{OLTC} and the target V_{target} .
- 291 • STEP# γ : the voltage violation at the LV side of transformer is verified. In fact, to avoid
292 excessive tap changes, the OLTC control changes if the voltage is outside or inside the
293 deadband $\pm DB$.
- 294 • STEP# $\delta 1$: in case of voltage violation (i.e., $|\Delta V_{\text{OLTC}}| > DB$) voltage counter $\alpha_{\text{OLTC}}(t)$ is
295 updated by adding or subtracting the quantity $\alpha_{\text{OLTC},\Delta t}$, as defined in (1):

$$296 \quad \alpha_{\text{OLTC}}(t) = \alpha_{\text{OLTC}}(t-1) \pm \alpha_{\text{OLTC},\Delta t}(t-1) \quad (1)$$

297 The increment $\alpha_{\text{OLTC},\Delta t}$ is proportional to the absolute value of ΔV_{OLTC} , as shown in (2):

$$298 \quad \alpha_{\text{OLTC},\Delta t}(t) = \frac{2 \cdot (|\Delta V_{\text{OLTC}}|)}{t_{\text{adm}} \cdot DB} \Delta t = \frac{2 \cdot (|V_{\text{OLTC}}(t) - V_{\text{bus,BT}}|)}{t_{\text{adm}} \cdot DB} \Delta t \quad (2)$$

299 where $\alpha_{\text{OLTC},\Delta t}$ is inversely proportional to DB and depends on the admitted voltage
300 violation time t_{adm} (whose effect will be shown in Fig.4). In the present work, the voltage
301 deadband DB is equal to half a tap ($DB = \Delta V_{\text{tap}}/2$). If the parameter $\alpha_{\text{OLTC}}(t)$ exceeds the
302 limits ± 1 , it is saturated at ± 1 .

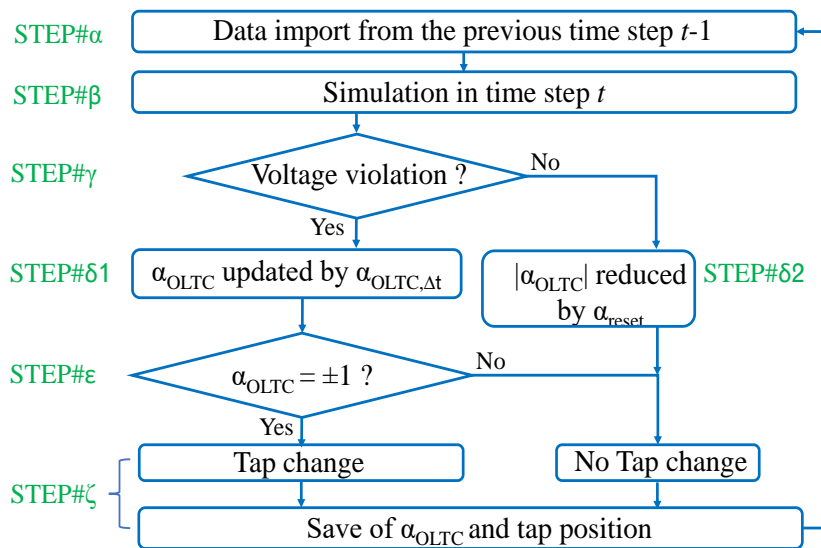
- 303 • STEP# $\delta 2$: in case of no voltage violation ($|\Delta V| < DB$), $\alpha_{\text{OLTC}}(t)$ is partially reset. This
304 partial reset is necessary to avoid unnecessary tap changes due to violations occurred

305 much earlier. For example, a temporary overvoltage occurred in the early morning should
 306 not lead to a tap change in the late afternoon. Thus, at each step without voltage violation,
 307 the parameter α_{reset} (over-under voltage parameter) is used to decrease the value of
 308 $\alpha_{\text{OLTC}}(t)$ according to (3):

$$309 \quad \alpha_{\text{OLTC}}(t) = \alpha_{\text{OLTC}}(t-1) \pm 1/\alpha_{\text{reset}} \quad (3)$$

310 The parameter α_{reset} represents the time (in minutes) necessary to reset the counter
 311 $\alpha_{\text{OLTC}}(t)$. In fact, after a number of time steps with no violations equal to $\Delta\alpha_{\text{OLTC}}$, the
 312 counter $\alpha_{\text{OLTC}}(t)$ is restored back to zero.

- 313 • STEP# ϵ : if $|\alpha_{\text{OLTC}}(t-1)|=1$, the tap position changes at the beginning of the next time step
 314 t . If $\alpha_{\text{OLTC}}(t)=1$, the tap increases $\text{tap}(t) = \text{tap}(t-1)+1$ for a lower voltage; if $\alpha_{\text{OLTC}}(t)=-1$,
 315 the tap decreases to obtain a higher voltage.
- 316 • STEP# ζ : in the last step, the updated value of $\alpha_{\text{OLTC},\Delta t}$, and the updated tap position to be
 317 used in the next simulation, are saved. It is noteworthy that, after a tap change, a minimum
 318 time $t_{\text{min,two,taps}}$ is waited before permitting another one to avoid fast tap oscillations.

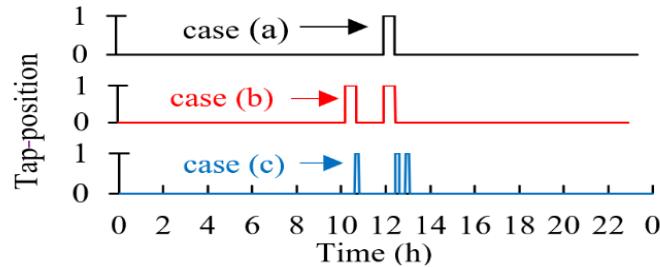


319
 320 Fig. 3. Procedure for the control of the OLTC.

321 2.3.1 Example of the effect of the change of the setup parameters for the OLTC

322 As mentioned in STEP# $\delta 1$, a key parameter to control the OLTC is the time t_{adm} ; it changes the

323 slew rate of the device limiting the number of tap changes N_{tap} . In fact, according to (2), $\alpha_{\text{OLTC},\Delta t}$
 324 and t_{adm} are inversely proportional. In conclusion, a high value of t_{adm} leads to a lower slew rate
 325 of the OLTC. This is confirmed by the example presented in Fig. 4, in which three simulations
 326 are presented. They are characterized by different parameters of proportional-integral control:
 327 in case (a), the parameters are $t_{\text{min,two,taps}}=30$ min, $t_{\text{adm}}=20$ min, $\alpha_{\text{reset}}=30$. In case (b) the setup
 328 is $t_{\text{min,two,taps}}=30$ min, $t_{\text{adm}}=5$ min and $\alpha_{\text{reset}}=40$; in case (c) the setup is $t_{\text{min,two,taps}}=10$ min,
 329 $t_{\text{adm}}=5$ min and $\alpha_{\text{reset}}=10$. For the sake of clarity, only the first phase is represented in Fig. 4.
 330 In case (a), during the whole day, the OLTC executes 2 tap changes, whereas in case (b) there
 331 are 4 tap changes. In the last case, the number of tap changes is the highest (six) because all the
 332 parameters are the lowest (have the lowest values). In cases (b) and (c), the OLTC is very
 333 sensitive due to the low t_{adm} . The small value of $t_{\text{min,two,taps}}$ in case (c) permits to perform more
 334 tap changes in a reduced time frame.



335
 336 Fig. 4. Tap position by varying $t_{\text{min,two,taps}}$, t_{adm} and α_{reset} .

337

338 3. Optimal Setups of Voltage Control Devices

339 The decision variables considered in this analysis are the parameters of the VCDs. The effects
 340 of these parameters on the voltage profiles of the LV grids under study, as well as the Joule
 341 losses in the lines and the number of tap changes of the OLTC, are taken into account and play
 342 a fundamental role in the optimization process. Section 3.1 describes the indicator used to
 343 evaluate the voltage deviations in the whole LV grid. Section 3.2 presents the complete lists of
 344 the parameters used for setting up the VCDs; these are the inputs parameters that are changed

345 in each simulation scenario. The scenarios are created to study the effect of the change in the
 346 inputs parameters on the optimization results. Finally, Section 3.3 presents the procedure to find
 347 the optimal setups.

348 3.1 Voltage indicators

349 The calculation of voltage indicators allows to evaluate the effectiveness of each type of voltage
 350 control. Among all the possible voltage indicators useful to calculate the quality of the voltage
 351 profiles, the most important used in the present work is the Voltage Deviations with Energy
 352 Flows (*VDEF*) [29]. It counts the sum of the squares of voltage deviations (with respect to a
 353 reference value V_{ref}) in each node k of the grid and at each time step t . Each deviation is
 354 multiplied by the energy $E_{k,t}$ to give more importance to the nodes and time steps in which the
 355 consumption is higher [37]. This sum is divided by the total energy consumed in the grid during
 356 the simulated period:

$$357 \quad VDEF = \frac{\sum_{t=1}^M \sum_{k=1}^{N_{nodes}} (V_{k,t} - V_{ref})^2 \cdot E_{k,t}}{\sum_{t=1}^M \sum_{k=1}^{N_{nodes}} E_{k,t}} \quad (4)$$

358 with M indicating the maximum number of time steps composing the timeframe T .

359

360 3.2 Input parameters of voltage control devices

361 According to [21], [29], [38], and this work, the variation of the input parameters (setup) of
 362 distributed PV inverters affects the three objective functions L_{tot} , N_{tap} and *VDEF* as follows:

- 363 • $V_{limit,max,PV}$: a reduction of this parameter leads to a restriction of the band delimited by
 364 $V_{range,max,PV}$ and $V_{limit,max,PV}$, and the decrease of the *VDEF* of the grid. However, L_{tot}
 365 increases due to the inductive power supplied to reduce the overvoltage.
- 366 • $V_{range,max,PV}$: a reduction of this parameter leads to a restriction of the target range
 367 delimited by $V_{range,min,PV}$ and $V_{range,max,PV}$. In this case, the PV inverters provide more
 368 inductive power to decrease the *VDEF* and to stabilize the voltage below the limit.

- 369 • $V_{\text{range,min,PV}}$: an increase of this parameter leads to a reduction of the target range between
 370 $V_{\text{range,min,PV}}$ and $V_{\text{range,max,PV}}$. In this way, L_{tot} increases, but the $VDEF$ decreases because
 371 the inverters provide more capacitive power to stabilize the voltage above the limit.
- 372 • $V_{\text{limit,min,PV}}$: an increase of this limit leads to a reduction of $VDEF$, but L_{tot} can increase if
 373 the inverters provide higher capacitive power to stabilize the voltage above the limit.

374 The effects of the variation of the setup parameters of the OLTC are described in the following
 375 list:

- 376 • V_{target} : it is the voltage goal for the OLTC. The variation of this parameter leads to a
 377 voltage variation in all the grid.
- 378 • t_{adm} : a reduction of this parameter leads to an increase of $\alpha_{\text{OLTC},\Delta t}$; thus, the number of tap
 379 changes N_{tap} increases leading to a reduction of $VDEF$.
- 380 • $t_{\text{min,two,taps}}$: an increase of this parameter leads to a reduction of N_{tap} because the tap
 381 changer cannot work for a longer time after a step. Thus, the $VDEF$ increases because of
 382 a reduced operation of the OLTC.
- 383 • α_{reset} : a high value of this parameter implies a lower slew rate of the OLTC; thus, a
 384 reduction of the N_{tap} and an increase of $VDEF$.

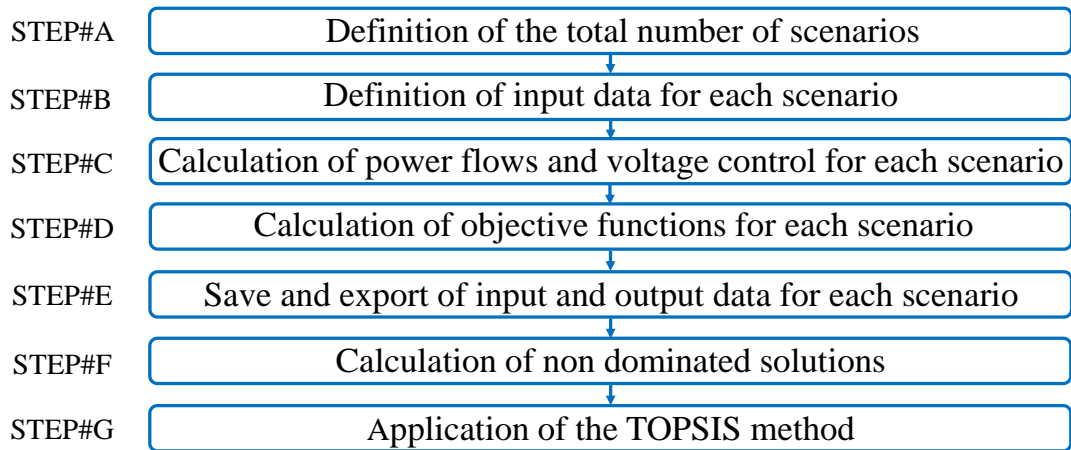
385 All the above parameters differ for every scenario and are randomly changed inside specific
 386 ranges. For the voltage limits of inverters, $V_{\text{limit,min,PV}} > 0.9$ and $V_{\text{limit,max,PV}} < 1.1$. According to
 387 Fig. 2, $V_{\text{range,max,PV}}$ and $V_{\text{range,max,PV}}$ lie within those limits.

388 For the OLTC, V_{target} is close to unity, t_{adm} and $t_{\text{min,two,taps}}$ are in the range 1÷30 min, and α_{reset}
 389 varies between 1 and 30.

390

391 3.3 Calculation of the optimal setups for voltage control

392 Fig. 5 shows the proposed procedure to study and compare different setups of the voltage
 393 control devices by solving the multi-objective problem.



394

395

Fig. 5. Procedure for the study of optimal setups of voltage control devices.

396

- STEP#A: the procedure starts with the selection of the total number of scenarios to be analyzed. It is an information that affects the simulation time.

397

398

- STEP#B: the inputs to be changed in each scenario are selected. They are the setup of the voltage control devices, e.g., the voltage limits of the capability curves of PV inverters and the parameters of the PI control. The complete list of the setup parameters was presented in the previous Section 3.2.

399

400

401

402

- STEP#C: the power flows are calculated, and the voltage control is performed. Each scenario has a different simulation performed according to the methodology explained in Section 2 for a timeframe T with time step t .

403

404

405

- STEP#D: the objective functions are calculated to perform the optimization. In the proposed procedure, the objective functions are the Joule losses for the whole grid L_{tot} , the number of tap changes N_{tap} , and the voltage indicator $VDEF$.

406

407

408

- STEP#E: all input and output data of each scenario are saved and organized for the next Pareto analysis.

409

410

- STEP#F: within all the sets of results, those that belong to the Pareto front are identified.

411

They represent the non-dominated solutions for which there is no objective function that

412

is simultaneously better for all the analyzed objective functions.

413 • STEP#G: the TOPSIS method [39] is applied to determine the ranking of the best
414 solutions that belong to the Pareto front. It is noted that the results obtained with TOPSIS
415 method depend on the weight assigned to each objective function. Moreover, the sum of
416 all weights must be 1.

417

418 **4. Case Studies and Grid Configurations**

419 The various aspects that refer to the preparation of the data for running the optimization
420 procedure are described below. Section 4.1 contains the description of the two grids under
421 analysis. Section 4.2 provides information about the measurement of generation and load
422 profiles used as inputs for the simulations. Section 4.3 shows how the combination of the two
423 grids and the measured profiles leads to the creation of different configurations. The resulting
424 configurations correspond to the two grids considered, with renewable energy generators
425 positioned in different nodes in the grid and with different nominal sizes.

426 *4.1 Description of the case studies*

427 The simulations are performed on two LV grids:

- 428 1. Grid#1 (20 lines, 21 nodes); contains a three-phase transformer (20 kV/400 V, rated
429 power $S_{\text{rated,tr}} = 400$ kVA, rated current $I_n = 570$ A, short-circuit impedance $Z_{\text{SC}} = 24$ m Ω
430 and short circuit power losses at 75°C $P_{\text{SC},75^\circ\text{C}} = 4.7$ kW).
- 431 2. Grid#2 (18 lines, 19 nodes); contains a three-phase transformer (20 kV/400 V, rated
432 power $S_{\text{rated,tr}} = 250$ kVA, rated current $I_n = 361$ A, short-circuit impedance $Z_{\text{SC}} \cong 38$ m Ω
433 and short circuit power losses at 75°C $P_{\text{SC},75^\circ\text{C}} = 3.4$ kW).

434 In both grids, the slack node #0 is the MV bus of the MV/LV substation. In all the lines, the
435 resistive component of the cables prevails over the inductive one. The LV grids have grounded
436 neutral and lines with three-pole underground cables, except for the overhead cables in

437 proximity of the transformer. The structure of each grid is shown in [29]. The transformer is
438 represented by the pi-model, neglecting the iron losses. The series impedance is calculated
439 starting from the transformer datasheets. The tap changer has a voltage step of 1.25% of the
440 nominal value and seven tap positions (-3,...,0,...,+3) corresponding to LV-side voltage
441 changing in the range 0.9625 – 1.0375 p.u. when the transformer is supplied at nominal primary
442 voltage.

443 *4.2 Load and generation profiles*

444 Load and generation profiles have been measured using the Data Acquisition System (DAS)
445 described in [40] and characterized by relative uncertainties equal to about 1%. The generation
446 profiles consist of active power values measured during a week in September, which adequately
447 represent an average generation along the year. These measured generation profiles are used as
448 a reference sample: the generation in each node is recreated by amplifying the measured profiles
449 without considering partial shading effects on the PV modules. On the contrary, the reactive
450 power profiles from the PV inverters are simulated according to the voltage control described
451 in the presented work. Regarding the load profiles, they are active and reactive power
452 absorptions of the aggregation of apartments and offices.

453 *4.3 Grid configurations*

454 In Grid#1, the ratio θ_{PV} between the maximum power produced by all the PV generators and
455 the maximum load in the whole grid is $\theta_{PV,grid1} \approx 46\%$ due to an overall PV nominal power at
456 AC side of 250 kVA. In Grid#2, this ratio is $\theta_{PV,grid2} \approx 50\%$ due to an overall PV nominal power
457 of 126 kVA. It is worth noting that the load and generation power peaks used to calculate these
458 ratios are not simultaneous. For these two reference grid configurations, simulations are carried
459 out by changing the position of load and generators or by increasing θ_{PV} . The increase of θ_{PV} is
460 obtained selecting generation profiles with higher production. For each configuration listed in

461 Table 1, the procedure for the study of optimal setups (Fig. 5) is applied and results are
 462 discussed in the next subparagraphs.

463 **Table 1. Grid Configurations**

Grid	Configuration	Description
1	CONF#1	Reference configuration for Grid#1
	CONF#2	Different positions of loads and generators
	CONF#3	Higher PV production peak - $\theta_{PV,grid1} \approx 55\%$
2	CONF#4	Reference configuration for Grid#2
	CONF#5	Different positions of loads and generators
	CONF#6	Higher PV production peak - $\theta_{PV,grid2} \approx 70\%$

464

465 5. Simulation Results

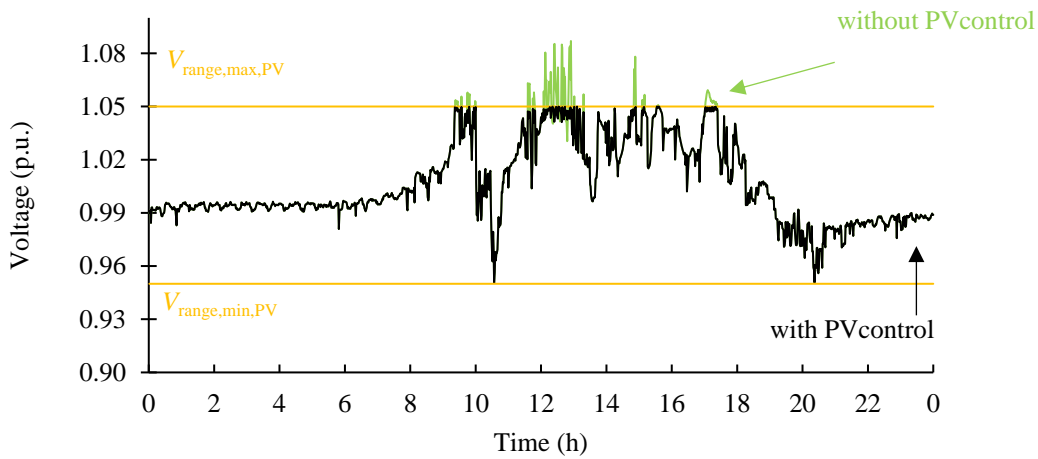
466 The results of the simulations performed are shown below. Section 5.1 presents examples of
 467 daily voltage profiles obtained by controlling the PV inverters and the OLTC, following the
 468 logics and procedures described in the previous sections. These examples are useful to better
 469 understand the effects of the different voltage controls. For this purpose, the proposed graphs
 470 show the controlled voltage profiles with respect to the same cases in which control is absent.
 471 After the examples, Section 5.2 and Section 5.3 present the aggregated results of the simulation
 472 of 6000 scenarios, each one with a different setup of the voltage controls. To compare the
 473 results, a TOPSIS solutions ranking is applied, and the best scenarios are found from the
 474 ranking. Finally, a sensitivity analysis is performed to analyze how the the ranking of the
 475 solutions changes by using different weights for the objective functions.

476

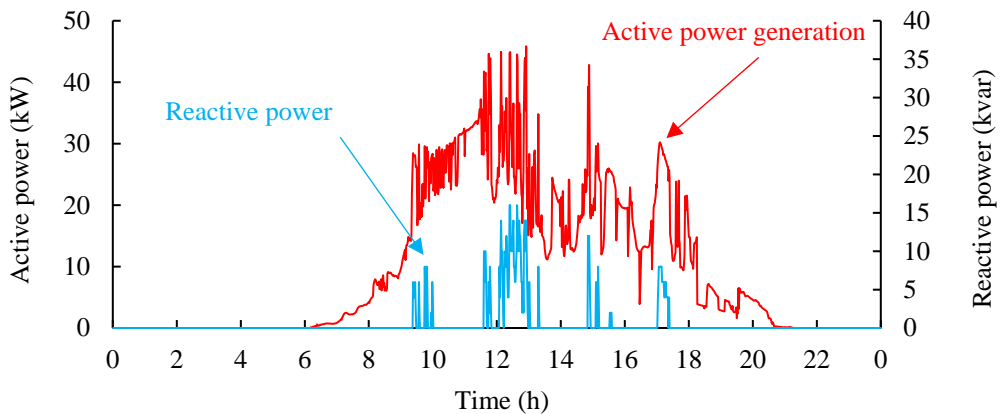
477 5.1 Examples of simulated voltage profiles obtained by controlling PV inverters and the OLTC

478 All types of voltage control are performed for a week with 1-minute time step. Fig. 6 shows a
 479 daily example of voltage profiles calculated without voltage control (CONF#1, day#1, node
 480 #18). In the figure, this profile can be compared with the one obtained in case of reactive power
 481 control from the PV inverter. Profiles refer to node #18, that is, the one with the highest
 482 impedance. The horizontal lines are the limits for the voltage control of the inverter. If the

483 voltage is higher than $V_{\text{range,max,PV}}$, the inverter provides inductive reactive power to stabilize the
 484 voltage below the limit border. In this example, between hours 12:00 and 14:00, the voltage is
 485 higher than the limit border due to the peak of PV production; thus, the inverter provides
 486 inductive power (peak \approx 15 kvar). No capacitive power is supplied because the voltage is never
 487 below $V_{\text{range,min,PV}}$. The active and reactive power profiles related to Fig. 6 are shown in Fig. 7.
 488 For the sake of clarity, all these profiles refer to the first phase of the unbalanced three phase
 489 system.



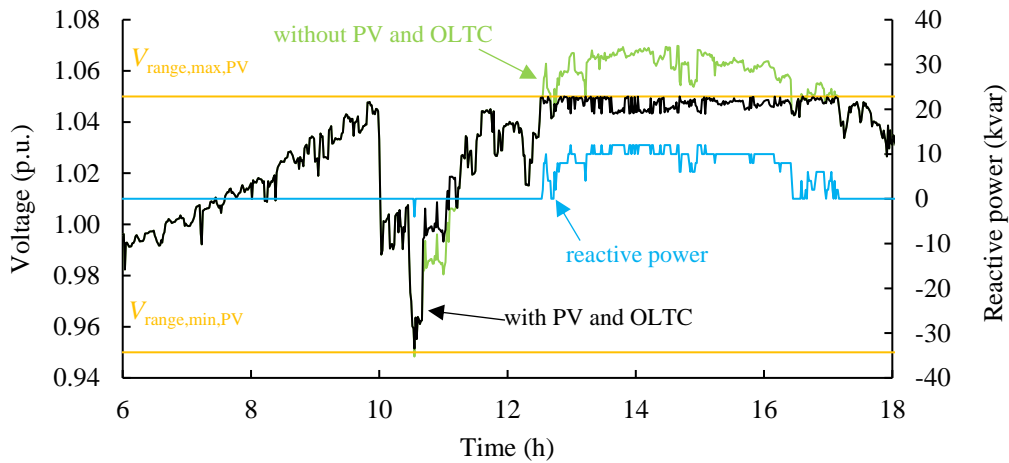
490
 491 Fig. 6. Example of daily voltage profile: no control vs. reactive power from PV inverters - CONF#1,
 492 day#1, node #18.



493
 494 Fig. 7. Active and reactive profiles related to the example in Fig. 6.

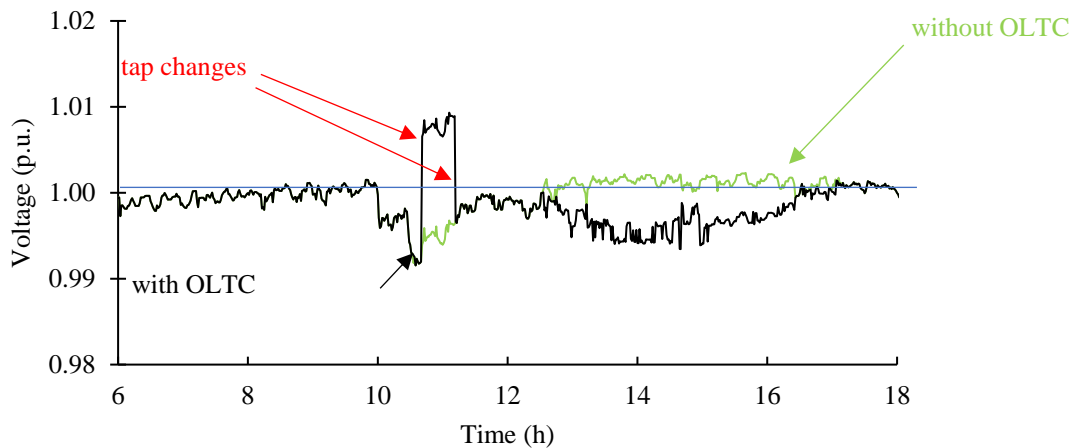
495 Fig. 8 shows another voltage profile calculated in case of voltage control performed from both
 496 PV generators and the OLTC (Grid#1, day#2, node #18). At hour 10:30, the load increases
 497 leading to an undervoltage; the PV power production is still too low, and inverters do not

498 contribute with capacitive power. The load increase influences the voltage at the PCC of the
 499 OLTC (Fig. 9); it decreases the tap to adjust the voltage. After ≈ 45 min, the OLTC returns to
 500 the previous position. After midday, the overvoltages are managed by the PV inverters, with no
 501 other tap changes.



502
 503
 504

Fig. 8. Example of daily voltage profile: no control vs. OLTC+PV operation - CONF#1, day#2, node #18.



505

506
 507

Fig. 9. OLTC operation related to the example in Fig. 8 - CONF#1, day#2, node #1 (LV side of the transformer).

508 Table 2 shows the values of the three objective functions $VDEF$, L_{tot} and N_{tap} in case of voltage
 509 control performed by PV inverters, with or without OLTC operation. All the results refer to the
 510 whole week under analysis. In Grid#1, the $VDEF$ decreases from $2.99 \cdot 10^{-4}$ to $2.90 \cdot 10^{-4}$ ($\approx -5\%$)
 511 due to 8 tap changes. In Grid #2, the $VDEF$ decreases from $1 \cdot 10^{-4}$ to $8.76 \cdot 10^{-5}$ due to 10 tap
 512 changes ($\approx -15\%$). In both examples, the OLTC operation does not interfere with inverters

513 leading to higher losses L_{tot} (in Grid#1 the increment is negligible).

514

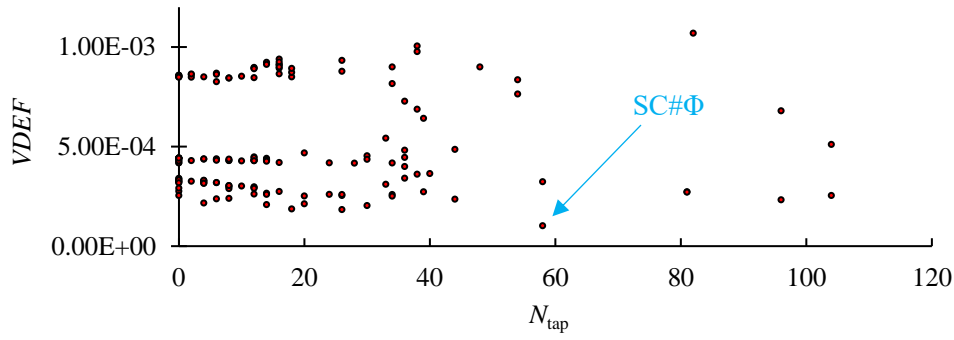
515

Table 2. Losses and V_{def} with PV inverters or/and OLTC

Grid	Objective function	Only PV inverters	PV inverters and OLTC
#1	L_{tot} (kWh)	171	171
	$VDEF$	$2.99 \cdot 10^{-4}$	$2.90 \cdot 10^{-4}$
	N_{tap} (phase 1)	-	8
#2	L_{tot} (kWh)	54	54
	$VDEF$	$1 \cdot 05^{-4}$	$8.16 \cdot 10^{-5}$
	N_{tap} (phase 1)	-	12

516 *5.2 TOPSIS solutions ranking*

517 The number of Scenarios (SC), simulated in the present work, is 1000 for each grid
518 configuration, corresponding to a total of 6,000 scenarios. Each scenario starts with a different
519 setup of the devices and includes a week of simulations with 1-min time step. For each grid
520 configuration, the input parameters of voltage control devices are varied according to Section
521 3.2. Fig. 10 shows the Pareto front related to the three objective functions obtained in CONF#1.
522 For the sake of simplicity, this figure does not show the third objective function L_{tot} . In the
523 Pareto front there is a Scenario (SC# Φ) with minimum value of $VDEF=1 \cdot 10^{-4}$, while $N_{tap} = 58$
524 and $L_{tot} = 674$ kWh are not the lowest. This particular case has very high losses with respect to
525 the average ≈ 150 kWh. Thus, a 3D view is necessary to better understand the scenario
526 distribution. Fig. 11 shows the 3D Pareto front. The SCs are divided in three groups in the front,
527 identified by three rectangles. One group is characterized by scenarios with higher voltage
528 deviations and lower losses. In the other two groups, $VDEF$ is lower due to higher use of
529 reactive power, leading to high L_{tot} . In every group, the number of tap changes is quite variable,
530 but in most cases is lower than 50.



531

532

Fig. 10. Pareto front of two of the three objective functions – CONF#1.

533

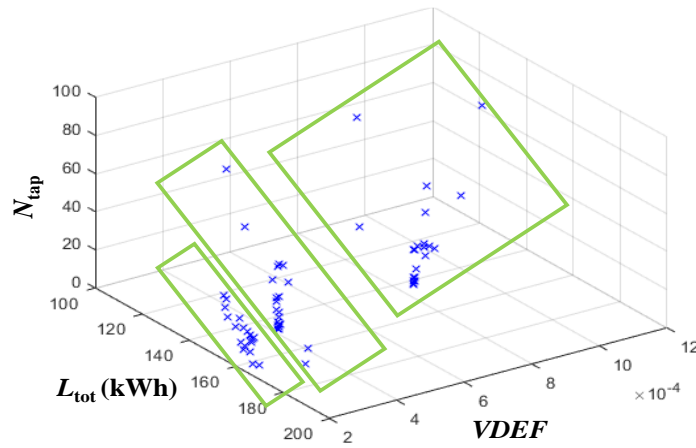
After the calculation of the 149 non-dominated solutions, the TOPSIS method is applied, and

534

the scenarios are ranked. In this case, the ranking weight for $VDEF$ is $w_{VDEF}=0.5$, for the losses

535

$w_{L_{tot}}=0.4$, and for the tap changes $w_{N_{tap}}=0.1$. Table 3 shows the resulting 5 best solutions.



536

537

Fig. 11. 3D Pareto front of the three objective functions – CONF#1.

538

Table 3. Best Solutions with $w_{VDEF}=0.5$, $w_{L_{tot}}=0.4$ and $w_{N_{tap}}=0.1$ - Configuration#1

Ranking	BS#1	BS#2	BS#3	BS#4	BS#5
$VDEF (\cdot 10^{-4})$	2.16	2.37	2.40	2.53	2.61
L_{tot} (kWh)	165	161	156	162	151.3
N_{tap}	4	6	8	0	12
$V_{limit,max,PV}$ (p.u.)	1.075	1.094	1.085	1.085	1.098
$V_{limit,min,PV}$ (p.u.)	0.920	0.909	0.923	0.905	0.919
$V_{range,max,PV}$ (p.u.)	1.072	1.092	1.075	1.056	1.065
$V_{range,min,PV}$ (p.u.)	0.986	0.982	0.981	0.975	0.972
V_{target} (p.u.)	1.003	1.002	1.003	1.001	1.002
t_{adm} (min)	29	14	19	30	13
$t_{min,two,taps}$ (min)	18	25	4	26	20
α_{reset}	24	29	8	29	14

539

The Best Scenario BS#1 has minimum $VDEF = 2.16 \cdot 10^{-4}$ and $N_{tap} = 4$. BS#2 has $VDEF =$

540

$2.37 \cdot 10^{-4}$ and $N_{tap} = 6$. The other scenarios have similar results, with losses between 165 and

541 151 kWh. The main difference is in the number of tap changes; the OLTC responsivity is mainly
542 influenced by t_{adm} . The key point is the setup of the inverters: the range $V_{range,max,PV} - V_{limit,max,PV}$
543 is small to limit the losses in the overvoltage management. Due to the reduced undervoltage in
544 the case studies, the $V_{limit,min,PV} - V_{range,min,PV}$ range is wide because it is less important for the
545 loss increase. By changing the importance of losses, and focusing on voltage quality, the
546 operation of inverter is boosted with a new set of weights, where w_{VDEF} is dominant, $w_{VDEF}=0.8$,
547 $w_{Ltot}=0.1$, and $w_{Ntap}=0.1$; the results are shown in Table 4. With this new set of weights, the
548 range $V_{range,max,PV} - V_{limit,max,PV}$ is always much higher than in Table 3. The OLTC operation
549 increases the voltage quality, mainly due to low values of t_{adm} .

550 **Table 4. Best Solutions with $w_{VDEF}=0.8$, $w_{Ltot}=0.1$ and $w_{Ntap}=0.1$ - Configuration#1**

Scenario Ranking	BS#1	BS#2	BS#3	BS#4	BS#5
$VDEF (\cdot 10^{-4})$	1.86	1.83	2.16	2.12	2.03
L_{tot} (kWh)	234	227	165	188	190
N_{tap}	18	26	4	20	30
$V_{limit,max,PV}$ (p.u.)	1.082	1.080	1.075	1.077	1.071
$V_{limit,min,PV}$ (p.u.)	0.925	0.924	0.920	0.911	0.918
$V_{range,max,PV}$ (p.u.)	1.056	1.050	1.073	1.051	1.050
$V_{range,min,PV}$ (p.u.)	0.997	0.988	0.986	0.982	0.982
V_{target} (p.u.)	0.998	1.003	1.003	1.002	1.004
t_{adm} (min)	25	12	29	9	19
$t_{min,two,taps}$ (min)	30	27	18	3	15
α_{reset}	16	21	24	3	3

551 **5.3 TOPSIS best solution in different grid configurations**

552 Table 5 shows the best solution obtained with TOPSIS for the different grid configurations.
553 CONF#1 is not included in Table 5, because data are already BS#1 in Table 4. Again, the
554 ranking weights are $w_{VDEF}=0.8$, $w_{Ltot}=0.1$ and $w_{Ntap}=0.1$.

555 **Table 5. TOPSIS Solution for Different Grid Configurations**

Configuration	#2	#3	#4	#5	#6
$VDEF (\cdot 10^{-4})$	2.00	2.23	5.32	4.52	1.01
L_{tot} (kWh)	444.5	275.1	57.9	24.7	101.1
N_{tap}	18	16	6	8	2
$V_{limit,max,PV}$ (p.u.)	1.072	1.082	1.075	1.079	1.082
$V_{limit,min,PV}$ (p.u.)	0.920	0.925	0.920	0.924	0.925
$V_{range,max,PV}$ (p.u.)	1.021	1.056	1.073	1.058	1.095
$V_{range,min,PV}$ (p.u.)	0.966	0.997	0.986	0.917	0.914
V_{target} (p.u.)	0.994	0.998	1.003	1.002	1.000

Configuration	#2	#3	#4	#5	#6
t_{adm} (min)	20	25	29	6	21
$t_{min,two,taps}$ (min)	28	30	18	18	25
α_{reset}	25	16	24	8	18

556

557 The best scenario in CONF#2 is particular, because the voltage target of the OLTC is generally
558 ≈ 1 . In this case, the target is lower leading to a high number of tap changes and high use of
559 reactive power with the highest losses. Accepting a worsening, CONF#3 (despite the high PV
560 injections) permits lower losses. In both cases, the setup of the OLTC is not the most responsive,
561 and the number of tap changes is always below 20. In Grid #2 (CONF#4, #5 and #6) the same
562 considerations can be applied.

563 5.4 Sensitivity analysis of the TOPSIS weights

564 Another sensitivity analysis has been carried out to analyze how the results change by using
565 different weights for the objective functions. Table 6 shows the results for the best scenario
566 obtained for each set of weights in CONF#1. The sets of weights WS#3 and WS#6 lead to the
567 same best scenario with the lowest $VDEF$, because w_{VDEF} is high. Thus, voltage control is the
568 most efficient with many tap changes and high reactive power and losses. On the contrary,
569 WS#4, WS#7 and WS#10 do not involve OLTC operation, with lower voltage quality. The
570 other sets are compromises, where the best solution should be selected by the grid management.

571

Table 6. Sensitivity Analysis of TOPSIS Weights - CONF#1

Weight Set	w_{VDEF}	$w_{L_{tot}}$	$w_{N_{tap}}$	$VDEF (\cdot 10^{-4})$	L_{tot} (kWh)	N_{tap}
1	0.5	0.4	0.1	2.16	165	4
2	0.4	0.4	0.2	2.16	165	4
3	0.8	0.1	0.1	1.86	234	18
4	0.2	0.4	0.4	2.76	152	0
5	0.3	0.6	0.1	2.40	156	8
6	0.9	0.05	0.05	1.86	234	18
7	0.3	0.2	0.5	2.53	162	0
8	0.7	0.2	0.1	2.16	165	4
9	0.1	0.1	0.8	2.53	162	0
10	0.3	0.1	0.6	2.53	162	0

572 6. Conclusions

573 The present study of voltage control in LV grids, performed by distributed PV inverters and
574 OLTC, aimed to find the optimal setups for their operation without any coordination, even
575 though a unique setup does not exist. Nevertheless, thanks to the result of the present work, the
576 Distribution System Operators are given reference values to decide the setup for the distributed
577 inverters to decide, considering their specific technical and economical constraints, how to face
578 voltage issues. The Distribution System Operators can stress the control setups to improve
579 voltage as much as possible, leading to higher Joule losses and maintenance cost, with less
580 issues for the users. On the contrary, they can use less strict voltage control to avoid excessive
581 increase in the costs.

582 The simulation results show how PV inverters can improve the voltage at their PCC adjusting
583 their reactive power. Nevertheless, in LV grids the effects are limited, as the grid is not very
584 inductive. On the contrary, the OLTC strongly affects the whole grid, but it cannot solve local
585 voltage violations. Indeed, since there is no method of communication with other nodes of the
586 grid, the OLTC may correct the voltage only at its PCC, where the voltage variation is low.
587 Nevertheless, as shown in this work, implicit cooperation without communication between the
588 OLTC and distributed PV inverters can be useful. The inverters will carry out a “*first*” partial
589 voltage control. Simulations have shown that inserting large voltage ranges (i.e., $V_{\text{limit,min,PV}} -$
590 $V_{\text{range,min,PV}}$ and $V_{\text{range,max,PV}} - V_{\text{limit,max,PV}}$) involves an important increase in reactive power and
591 losses to obtain a benefit on voltage. A large range with $V_{\text{range,max,PV}} = 1.05$ and $V_{\text{limit,max,PV}} \approx 1.08$
592 generally leads to a large use of reactive power and many tap changes (an average of ≈ 20
593 taps/day) to improve voltage with a resulting average value of $VDEF \approx 2.14 \cdot 10^{-4}$. Thus, for an
594 optimal compromise between losses, voltage violations and lifespan increase of the OLTC, the
595 ranges should be limited. Thus, the OLTC should solve the most serious voltage violations
596 working as a “*second*” voltage controller. A lower range with $V_{\text{range,max,PV}} = 1.07$ and $V_{\text{limit,max,PV}}$

597 ≈ 1.08 lead to a lower use of reactive power, and less tap changes (an average of ≈ 7 taps/day) to
598 improve voltage; as a result the quality of voltage profiles is lower, with an average value of
599 $VDEF \approx 1.83 \cdot 10^{-4}$. With respect the previously mentioned larger range $V_{\text{range,max,PV}} - V_{\text{limit,max,PV}}$,
600 there is a drop in voltage quality of about 20%. The control by inverter and OLTC leads to
601 better results when values of t_{adm} and $t_{\text{min,two,taps}}$ are smaller. In this way, the control is more
602 responsive to voltage variations. Therefore, the number of tap changes increases, and voltage
603 deviation is reduced. For local voltage problems not solved by the studied control devices, the
604 voltage quality could be improved by decreasing the impedance up to their PCC.
605 Moreover, the present work has presented the procedure used to obtain the above-described
606 results, in different setup scenarios and grid configurations. For each configuration, the Pareto
607 analysis provides the non-dominated solutions. A TOPSIS analysis is included in the procedure
608 to rank the scenarios. Finally, sensitivity analysis has been executed to evaluate how the results
609 change according to the weights assigned to each objective function.

610 7. References

- 611 1. O.S. Nduka, L.P. Kunjumammed, B.C. Pal, A. Majumdar, Y. Yu, S. Maiti, A.R. Ahmad, Field Trial of
612 Coordinated Control of PV and Energy Storage Units and Analysis of Power Quality Measurements, *IEEE*
613 *Access*, vol. 8, pp. 1962–1974, 2020.
- 614 2. M. Pau, E. De Din, F. Ponci, P.A. Pegoraro, S. Sulis, C. Muscas, Impact of uncertainty sources on the voltage
615 control of active distribution grids, *2021 International Conference on Smart Energy Systems and*
616 *Technologies (SEST)*, pp. 1-6, 2021.
- 617 3. D. Zhang, J. Li, D. Hui, Coordinated Control for Voltage Control of Distribution Network Voltage Control
618 by Distributed Energy Storage Systems, *Prot. and Contr. of Mod. Pow. Sys.*, vol. 3(1), pp. 1–8, 2018.
- 619 4. L. Del Rio Etayo, P. Cirujano, P. Lauzevis, G. Perez De Nalclares, A. Soto, A. Ulasenka, A new smart
620 distribution transformer with OLTC for low carbon technologies integration, *24th Int. Conf. on Electricity*
621 *Distribution*, paper no. 0832, Glasgow (UK), 12-15 June 2017.
- 622 5. A. Selim, M. Abdel-Akher, M.M. Aly, S. Kamel, T. Senjyu, Fast Quasi-static Time-series Analysis and
623 Reactive Power Control of Unbalanced Distribution Systems, *International Transactions on Electrical*
624 *Energy Systems*, vol. 29(1), ref. E2673, 2019.

- 625 6. M. Chamana, B.H. Chowdhury, F. Jahanbakhsh, Distributed Control of Voltage Regulating Devices in the
626 Presence of High PV Penetration to Mitigate Ramp-Rate Issues, *IEEE Trans. on Smart Grid*, vol. 9(2), pp.
627 1086–1095, 2018.
- 628 7. N. Daratha, B. Das, J. Sharma, Coordination Between OLTC and SVC for Voltage Control in Unbalanced
629 Distribution System Distributed Generation, *IEEE Trans. on Power Systems*, vol. 29(1), pp. 289–299, 2014.
- 630 8. J. Ma, H. Ye, L. Haifeng, Z. Li, P. Han, Z. Lin, J. Shi, Research on Source-Network Coordination Voltage
631 Control Strategy of Photovoltaic Power Plant Considering the Stability of Inverter Port Voltage, *E3S Web of*
632 *Conferences*, vol. 143, ref. 2018, 2020.
- 633 9. E.M. Darwish, H.M. Hasanien, A. Atallah, S. El-Debeiky, Reactive Power Control of Three-phase Low
634 Voltage System Based on Voltage to Increase PV Penetration Levels, *Ain Shams Engineering Journal*, vol.
635 9(4), pp. 1831–1837, 2018.
- 636 10. V.B. Pamshetti, S.P. Singh, Optimal Coordination of PV Smart Inverter and Traditional Volt-VAR Control
637 Devices for Energy Cost Savings and Voltage Control, *International Transactions on Electrical Energy*
638 *Systems*, vol. 29(7), 2019.
- 639 11. M. Chamana and B.H. Chowdhury, Optimal Voltage Control of Distribution Networks With Cascaded
640 Voltage Regulators in the Presence of High PV Penetration, *IEEE Trans. on Sustainable Energy*, vol. 9(3),
641 pp. 1427–1436, 2018.
- 642 12. R. Tonkoski, L.A.C. Lopes, T.H.M. El-Fouly, Droop-based Active Power Curtailment for Overvoltage
643 Prevention in Grid Connected PV Inverters, *2010 IEEE Int. Symp. on Industrial Electronics*, pp. 2388–2393,
644 2010.
- 645 13. S. M. Rostami, M. Hamzeh, Reactive Power Management of PV Systems by Distributed Cooperative Control
646 in Low Voltage Distribution Networks, *2021 29th Iranian Conference on Electrical Engineering (ICEE)*,
647 2021, pp. 412-417.
- 648 14. A.M. Howlader, S. Sadoyama, L.R. Roose, S. Sepasi, Distributed voltage control using Volt-Var controls of
649 a smart PV inverter in a smart grid: experimental study, *Renew. Energy*, vol. 127, pp. 145–157, 2018.
- 650 15. A.M. Howlader, S. Sadoyama, L.R. Roose, S. Sepasi, Distributed Voltage Control Method Using Volt-Var
651 Control Curve of Photovoltaic Inverter for a Smart Power Grid System, *2017 IEEE 12th Int. Conf. on Power*
652 *Electronics and Drive Systems (PEDS)*, pp. 630–634, 2017.
- 653 16. Z. Zhang, Y. Mishra, C. Dou, D. Yue, B. Zhang, Y.C. Tian, Steady-State Voltage Control With Reduced
654 Photovoltaic Power Curtailment, *IEEE Journal of Photovoltaics*, vol. 10(6), pp. 1853–1863, 2020.
- 655 17. S. Wang, L. Du, X. Fan, Q. Huang, Deep Reinforcement Scheduling of Energy Storage Systems for Real-
656 Time Voltage Regulation in Unbalanced LV Networks With High PV Penetration, *IEEE Trans. on*
657 *Sustainable Energy*, vol. 12, no. 4, pp. 2342-2352, Oct. 2021.
- 658 18. F. Marra, G. Yang, C. Traeholt, J. Ostergaard, E. Larsen, A Decentralized Storage Strategy for Residential
659 Feeders With Photovoltaics, *IEEE Trans. on Smart Grid*, vol. 5, pp. 974–981, 2014.
- 660 19. M.N. Kabir, Y. Mishra, G. Ledwich, Z.Y. Dong, K.P. Wong, Coordinated Control of Grid-Connected
661 Photovoltaic Reactive Power and Battery Energy Storage Systems to Improve the Voltage Profile of a
662 Residential Distribution Feeder, *IEEE Trans. on Industrial Informatics*, vol. 10(2), 967–977, 2014.

- 663 20. N. Efkarpidis, T. De Rybel, J. Driesen, Optimization control scheme utilizing small-scale distributed
664 generators and OLTC distribution transformers, *Sustainable Energy, Grids and Networks*, vol. 8, pp. 74–84,
665 2016.
- 666 21. A. Ciocia, G. Chicco, F. Spertino, Benefits of On-Load Tap Changers Coordinated Operation for Voltage
667 Control in Low Voltage Grids with High Photovoltaic Penetration, *2020 International Conference on Smart
668 Energy Systems and Technologies (SEST)*, 2020.
- 669 22. D.G. Infield, M. Thomson, Network power-flow analysis for a high penetration of distributed generation,
670 *2006 IEEE PES General Meeting*, 2006.
- 671 23. J. Wang, X. Zhu, D. Lubkeman, N. Lu, N. Samaan, B. Werts, Load Aggregation Methods for Quasi-Static
672 Power Flow Analysis on High PV Penetration Feeders, *2018 IEEE/PES Transmission and Distribution
673 Conference and Exposition (T&D)*, pp. 1-5, 2018.
- 674 24. M. de Montigny et al., Multiagent Stochastic Simulation of Minute-to-Minute Grid Operations and Control
675 to Integrate Wind Generation Under AC Power Flow Constraints, *IEEE Trans. on Sustainable Energy*, vol.
676 4(3), pp. 619-629, 2013.
- 677 25. C. Plath, M. Putter, OMICRON electronics GmbH, Dynamic analysis and testing of On-Load Tap Changer
678 with dynamic resistance measurement, Available online (accessed 31 March 2022):
679 <https://www.omicronenergy.com/download/file/a207466e7bc405ecd22dbec942a41199/>
- 680 26. G.R. Chandra Mouli, P. Bauer, T. Wijekoon, A. Panosyan, E. Bärthlein, Design of a Power-Electronic-
681 Assisted OLTC for Grid Voltage Regulation, *IEEE Trans. on Power Delivery*, vol. 30(3), pp. 1086-1095,
682 2015.
- 683 27. D. Dohnal, On-load tap-changers for power transformers, Available online (accessed 31 March 2022):
684 [https://www.reinhausen.com/fileadmin/downloadcenter/company/publikationen/f0126405_on-load_tap-
685 changers_for_power_transformers.pdf](https://www.reinhausen.com/fileadmin/downloadcenter/company/publikationen/f0126405_on-load_tap-changers_for_power_transformers.pdf)
- 686 28. D. Shirmohammadi, H.W. Hong, A. Semlyen, G.X. Luo, A Compensation-based Power Flow Method for
687 Weakly Meshed Distribution and Transmission Networks, *IEEE Trans. on Power Systems*, vol. 3(2), pp.
688 753–762, 1988.
- 689 29. A. Ciocia, V.A. Boicea, G. Chicco, P. Di Leo, A. Mazza, E. Pons, F. Spertino, N. Hadj-Said, Voltage Control
690 in Low-Voltage Grids Using Distributed Photovoltaic Converters and Centralized Devices, *IEEE Trans. on
691 Industry Applications*, vol. 55(1), pp. 225–237, 2019.
- 692 30. Italian Electrotechnical Committee (CEI), Reference technical rules for the connection of active and passive
693 users to the LV electrical Utilities, CEI Standard 0-21, December 2012 (In Italian).
- 694 31. A. Molina-Garcia, R.A. Mastromauro, T. Garcia-Sanchez, S. Pugliese, M. Liserre, S. Stasi, Reactive Power
695 Flow Control for PV Inverters Voltage Support in LV Distribution Networks, *IEEE Trans. on Smart Grid*,
696 vol. 8(1), pp. 447–456, 2017.
- 697 32. L. Collins, J.K. Ward, Real and Reactive Power Control of Distributed PV Inverters for Overvoltage
698 Prevention and Increased Renewable Generation Hosting Capacity, *Renewable Energy*, vol. 81 pp. 464–471,
699 2015.
- 700 33. A.F. Murtaza, M. Chiaberge, F. Spertino, U. T. Shami, D. Boero, M. De Giuseppe, MPPT technique based
701 on improved evaluation of photovoltaic parameters for uniformly irradiated photovoltaic array, *Electric
702 Power Systems Research*, vol. 145, pp. 248-263, 2017.

- 703 34. F. Spertino, J. Ahmad, A. Ciocia, P. Di Leo, A technique for tracking the global maximum power point of
704 photovoltaic arrays under partial shading conditions, *2015 IEEE 6th International Symposium on Power*
705 *Electronics for Distributed Generation Systems (PEDG)*, pp. 1-5, 2015.
- 706 35. D. Zeng, J. Guo, M. Ding, D. Geng, Fault ride-through capability enhancement by adaptive voltage support
707 control for inverter interfaced distributed generation, *2015 5th International Conference on Electric Utility*
708 *Deregulation and Restructuring and Power Technologies (DRPT)*, pp. 1924-1928, 2015.
- 709 36. D. Iioka, H. Saitoh, Enhancement of fault ride through capability using constant current control of
710 photovoltaic inverters, *2016 IEEE Innovative Smart Grid Technologies - Asia (ISGT-Asia)*, pp. 1083-1088,
711 2016.
- 712 37. E. Carpaneto, G. Chicco, M. De Donno, R. Napoli, Voltage controllability of distribution systems with local
713 generation sources, *Bulk Power System Dynamics and Control*, Cortina d'Ampezzo, Italy, August 22-27,
714 2004, pp. 261–273.
- 715 38. A. Ciocia, G. Chicco, P. Di Leo, M. Gai, A. Mazza, F. Spertino, N. Hadj-Said, Voltage control in low voltage
716 grids: A comparison between the use of distributed photovoltaic converters or centralized devices, *Proc. 2017*
717 *IEEE IEEEIC / I&CPS Europe*, pp. 1-6.
- 718 39. D.L. Olson, Comparison of weights in TOPSIS models, *Math. Comput. Model.*, vol. 40, no. 7-8, pp. 721–
719 727, 2004.
- 720 40. F. Spertino, A. Ciocia, P. Di Leo, R. Tommasini, I. Berardone, M. Corrado, A. Infuso, M. Paggi, A Power
721 and Energy Procedure in Operating Photovoltaic Systems to Quantify the Losses According to the Causes,
722 *Solar Energy*, vol. 118, pp. 313–326, 2015.